Velocity-dependent total scattering cross sections for $Ar(^3P_{2,0})$ on H_2O

K. Wang, J. Li, K. A. Hardy, and J. W. Sheldon
Physics Department, Florida International University, Miami, Florida 33199
(Received 28 June 1993)

Single-beam attenuation measurements of the velocity-dependent integral scattering cross sections for $Ar(^3P_{2,0})+H_2O$ are reported. The data are corrected for the finite angular resolution of the apparatus and the thermal motion of the target molecules. The measured total cross sections, which range from 505 $Å^2$ at 0.708 km/s to 236 $Å^2$ at 4.58 km/s, are analyzed semiclassically to obtain spherically averaged potential parameters and an upper limit to the inelastic cross section.

PACS number(s): 34.50.−s, 34.40.+n

I. INTRODUCTION

A study of the velocity-dependent total scattering cross sections of metastable $Ar(^3P_{2,0})$ (Ar^*) on water vapor is presented. Quenching reactions have been investigated for Ar^*+H_2O [1–9], but to our knowledge there have been no measurements of total scattering cross section for this collision pair. The interaction is expected to be extremely anisotropic, with the Ar^* being attracted to the oxygen atom and repelled by the hydrogens [10]. Faubel and Toennies [11] have pointed out that for anisotropic systems, total scattering cross sections are mainly sensitive to the spherical part of the long-range potential.

II. APPARATUS

The present measurement is made using a single-beam apparatus with water vapor in the target cell. The molecular-beam apparatus used in this work has been described previously [12,13]. Metastable atoms effusing from a gas discharge are collimated, chopped and velocity analyzed by the time-of-flight (TOF) method. All products of the gas discharge except ground and metastable excited state atoms and photons are removed from the beam by sweep plates which maintain an electric field of 1000 V/cm normal to the beam path. The beam velocity resolution varies from 2% at the lowest relative velocities to 5% at the highest velocities. No separation of the two metastable states was attempted. However, in a similar discharge source [14] the $^3P_2$ states were shown to dominate by about 6–1 over the $^3P_0$ states.

Deionized, triple-distilled H_2O was alternately frozen at 77 K, pumped to about 10^{-5} Torr and thawed through several cycles before being used as the target vapor source. The target gas was supplied to the collision cell through a manifold which was kept at a pressure of 4.6 Torr by maintaining the liquid reservoir at 273 K. Water vapor flow to the collision cell was controlled by a metering valve, and the pressure in the cell was measured by two electronic capacitance manometers, the calibration of one of these being traceable to NIST. The pressure measurement was corrected for the difference in temperature between the capacitance manometers and the target gas cell. A TOF distribution was counted for 390 s with target gas (H_2O vapor) in the collision cell after which a solenoid valve downstream of the metering valve was closed by the computer. Following a suitable delay (120 s) to pump out the water vapor, the unattenuated TOF distribution was recorded. The computer continued to cycle the solenoid valve and alternately count the two TOF distributions, thereby averaging out long term drifts in the metastable beam intensity. The beam geometry has an angular resolution, θ_r, of 0.52 mrad by the Kusch criterion [15], and corrections for the finite angular resolution of the apparatus were applied as described below.

Effective total cross sections were calculated for each time channel using Beer's Law. The average relative velocity, g, and the apparent total cross sections, $Q_{ta}(g)$, were obtained from these effective values, the beam velocity, v_A, and the most probable velocity of the target molecules, v_p, by computing the correction for the velocity distribution of the target molecules following the method of Lang, Lilenfeld, and Kinsey [16].

The correction ΔQ for the finite angular resolution of the apparatus follows von Busch [17] and has been discussed elsewhere [18]. It is given by

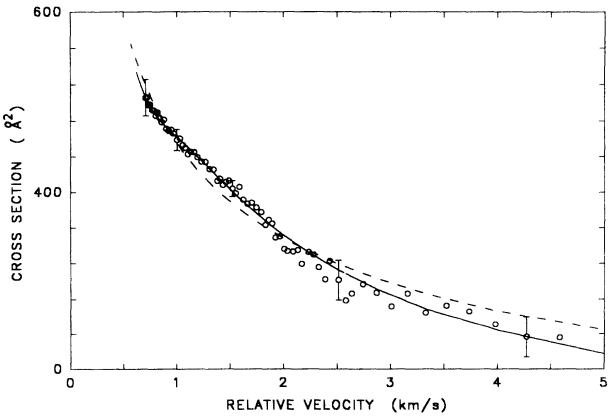

FIG. 1. Total cross section data corrected for finite angular resolution and thermal motion of the target molecules. The solid curve $Q_t(g)$ is calculated using Eqs. (3a)–(3e) and the parameters in Table I. The dashed curve $Q_L(g)$ is the Landau-Lifshitz cross section calculated using Eq. (3b) and the parameters in Table I.

$$\Delta Q=\frac{\alpha Q_{ta}^{3/2}}{1-\frac{3}{2}\alpha Q_{ta}^{1/2}}\ , \tag{1}$$

where

$$\alpha=0.265\,84\theta_r k\left[1+0.374\left[\frac{v_p}{v_A}\right]^2\right]$$

and k is the Ar* beam wave number, $m_A v_A/\hbar$. Our measured total scattering cross sections are then obtained from

$$Q_t(g)=Q_{ta}(g)+\Delta Q(g) \tag{2}$$

and presented in Fig. 1. In addition to the counting errors indicated by the error bars, a systematic error of up to 5% is possible due to the pressure measurement.

III. SEMICLASSICAL ANALYSIS

The data have been fitted by a nonlinear least-squares procedure to the semiclassical functions [19]

$$Q_t(g)=Q_L(g)+Q_g(g)\ , \tag{3a}$$

where

$$Q_L=p_1X^{p_2}\ , \tag{3b}$$

$$Q_g=D_a A_g\sin(\theta_g)\ , \tag{3c}$$

$$\theta_g=p_3+p_4X+p_5X^3\ , \tag{3d}$$

$$A_g=p_6X^{-1/2}+p_7X^{3/2}\ , \tag{3e}$$

and $X=g_0/g$ with the arbitrary reference velocity, $g_0=1.00$ km/s. The parameters p_1, p_6, and p_7 are used here in Å^2 and the other p's are dimensionless. The glory damping function, D_a is, in the semiclassical approximation, related to the imaginary part of the optical phase shift for the glory angular momentum, δ_g by [19]

$$D_a=e^{-2\delta_g}\ . \tag{4}$$

If an intermolecular potential $V(r)$ of the form

$$V(r)=\frac{n\epsilon}{n-s}\left[\left[\frac{s}{n}\right]\left[\frac{r_m}{r}\right]^n-\left[\frac{r_m}{r}\right]^s\right] \tag{5}$$

is used, where ϵ is the well depth in meV and r_m is the position of the well minimum in Å, then the long-range attractive term gives [20]

$$p_2=2/(s-1)$$

and

$$p_1=W(s)\left[\frac{1}{\hbar g_0}\frac{\epsilon r_m^s}{1-\frac{s}{n}}\right]^{2/(s-1)}\ , \tag{6}$$

where $\hbar g_0=6.595$ meV Å and

$$W(s)=2\pi^{s/(s-1)}\cos[\pi/(s-1)]\Gamma((s-3)/(s-2))\times\left[\frac{\Gamma((s-1)/2)}{\Gamma(s/2)}\right]^{2/(s-1)}\ .$$

The experimentally determined location of the glory maximum (which is assumed to be the first glory maximum), X_1 can be used in $\xi=5\pi(8a_1X_1)^{-1}$, [$a_1=0.4216$ (Ref. [21])] and the potential well depth $-\epsilon$ and location r_m are then obtained from p_1, p_2, and ξ using [20]

$$\epsilon=\hbar g_0\left[1-\frac{1}{n}-\frac{2}{np_2}\right]^{-p_2/2}\sqrt{W(s)/p_1}[\xi/2]^{(p_2+2)/2} \tag{7}$$

and

$$r_m=\frac{\xi\hbar g_0}{2\epsilon}\ . \tag{8}$$

The other p_i's are given in terms of ϵ and r_m using the semiclassical expansion by Bernstein and LaBudde [21]. The parameters in Eq. (3d) are $p_3=-3\pi/4$, $p_4=2\xi a_1$, and $p_5=2\xi E_0 A_1$, where $A_1=-0.1655$ and $E_0=\epsilon/\epsilon_{t0}$. The reference translational energy $\epsilon_{t0}=(\frac{1}{2})\mu g_0^2=64.8$ meV using μ, the reduced mass of the collision pair.

The parameters in Eq. (3e) are

$$p_6=B_0(2\pi r_m)^{3/2}\left[\frac{\hbar g_0}{\epsilon c_1}\right]^{1/2} \tag{9}$$

and

$$p_7=p_6H_1E_0\ , \tag{10}$$

where $B_0=0.946$, $c_1=25.4$, and $H_1=3.267$ (Ref. [21]). The calculation of a_1, A_1, B_0, c_1, and H_1 parameters was carried out by Bernstein and LaBudde [21] for a Lennard-Jones potential, but these parameters were shown to be nearly constant for "reasonable" potentials. In the present case, Eq. (5) with $n=12$ should fit the reasonable potential criteria.

For the present collision pair the glory oscillations are damped by inelastic events. The imaginary glory phase shift which determines the glory damping [Eq. (4)] is given here by the empirical expression

$$\delta_g=\delta_{g0}(1+D_1X+D_2X^2)\ . \tag{11}$$

In the initial data fitting procedure, the free parameters were p_1, p_2, X_1, δ_{g0}, D_1, and D_2, however, it was found that the best fit was obtained with $\delta_g=\delta_{g0}$ and D_1 and D_2 held at zero. Numerical experiments also demonstrated that the results were not very sensitive to n, which was therefore held fixed at 12. The best fit values of the four remaining free parameters and their standard deviations (calculated from the error bars indicated on Fig. 1,

TABLE I. Semiclassical parameters.

δ_{g0}	1.352±0.032
X_1	0.762±0.006
p_1	455.0±22.0 Å^2
p_2	0.387±0.001
s	6.17±0.01
ϵ	3.76±0.09 meV
r_m	5.31±0.13 Å

following the method of Shnidman [22]) are reported in Table I. The potential parameters ϵ, r_m, and s calculated from the fitting parameters are also presented in Table I. There may be some additional error in these parameters, since a systematic error of up to 5% is possible in the pressure measurement.

IV. RESULTS

The total cross sections, Q_t, computed from Eqs. (3) using the parameters of Table I are represented by the solid curve and compared to the experimental data in Fig. 1. Also shown is the Landau-Lifshitz cross section [20], Q_L. The glory part of the calculated cross section, Q_g [Eqs. (3c)–3(e)] is compared to the experimental data with the long-range attractive term subtracted ($Q_{gx}=Q_t-Q_L$) in Fig. 2.

The resulting values of the free parameters given in Table I are used in Eqs. (7) and (8) to get $\epsilon=3.76\pm0.09$ meV and $r_m=5.31\pm0.13$ Å for the Ar^*+H_2O well. These results represent an average over all orientations of the H_2O molecule. The long-range potential is typically described by

$$V(r)=-\frac{C_6}{r^6}-\frac{C_8}{r^8}-\frac{C_{10}}{r^{10}} ,$$

however, since $s=6.17$, there are only small contributions from the r^{-8} and r^{-10} terms. The semiclassical analysis used here does not provide a route to determining the individual C_6, C_8, and C_{10}.

V. DISCUSSION

The observed attenuation of the glory amplitude can be used to estimate an upper limit to the total inelastic cross section, Q_i, using an argument due to Kerstel *et al.* [19]. Classically,

$$Q_i=\int_0^\infty 2\pi P(b)b\,db .$$

The opacity function, $P(b(l))$ is generally a monotonically decreasing function with increasing angular momentum, l, which drops rapidly beyond the glory angular momentum, l_g (Ref. [23]), and semiclassically, $l_g\approx 2\epsilon_{t0}b_g(\hbar g_0)^{-1}$, therefore

$$Q_i\le \pi b_g^2 P(b_g)=Q_{\rm lim} , \tag{12}$$

where [19]

$$P(b_g)=1-e^{-4\delta_g} . \tag{13}$$

Since δ_g, and consequently $P(b_g)$, is determined here experimentally from the glory damping, it will include damping due to the anisotropy of the potential [24,25] as well as damping due to reactions and other inelastic processes. Therefore $Q_{\rm lim}$ should be an upper bound to the inelastic cross section. $Q_{\rm lim}$ is obtained from Eqs. (12) and (13) and the expansion [21]

$$b_g=(B_0+B_1E_0X^2+B_2E_0^2X^4)r_m , \tag{14}$$

where $B_1=0.3657$ and $B_2=-0.277$. This estimate of $Q_{\rm lim}$ is compared in Fig. 3 with measured Ar^*+H_2O quenching cross sections, $Q_q(g)$. An error in $Q_{\rm lim}$ of ±5 Å^2 is possible due to the fitting errors in the parameters reported in Table I.

Penning ionization of H_2O by Ar^* is energetically forbidden, and associative ionization in the present energy range is less than 0.25 Å^2 (Ref. [3]). The dissociative quenching contribution to the inelastic cross section is the result of the two reaction channels [7,8]

$$Ar^*+H_2O\rightarrow \begin{cases} Ar+OH+H, & \text{(14a)} \\ Ar+2H+O. & \text{(14b)} \end{cases}$$

Tabayashi and Shobatake [8] obtain for the reaction (14a)

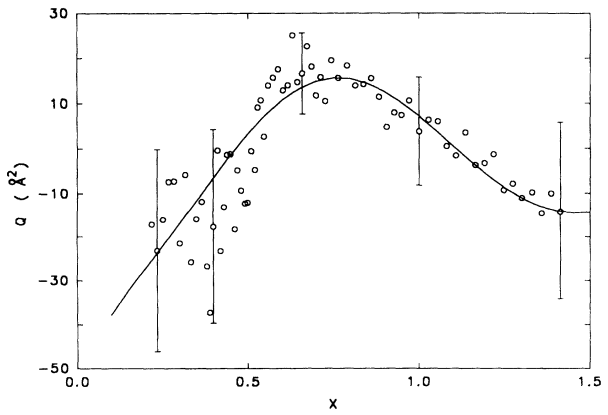

FIG. 2. The glory contribution to the total cross section. The same data as shown in Fig. 1, but, to emphasize the glory oscillation, $Q_L(g)$ from Eq. (3b) has been subtracted and plotted versus $X=g_0/g$. The curve is calculated from Eqs. (3c)–(3e) using the parameters in Table I.

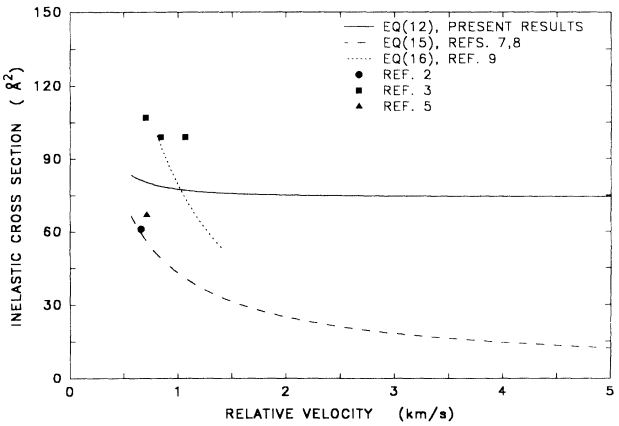

FIG. 3. Inelastic cross section measurements. The present measurements produce the upper bound, $Q_{\rm lim}$, which is calculated using the experimental results in Table I and Eq. (12). Other measurements shown are Bourène and Le Calvé [2], Sheldon and Muschlitz [3], and Velazco, Kolts, and Setser [5]. The long dashed curve, computed from Eq. (15), represents a combination of the measurements of Tabayashi and Shobatake [8] and Balamuta and Golde [7]. The short dashed curve, computed from Eq. (16), represents the measurements of Novicki and Krenos [9].

$$Q_{iA}(g)=23.2/g^{0.78} ,$$

where $Q_{iA}(g)$ is the inelastic cross section in $Å^2$ due to reaction (14a) and g is in km/s. Parr and Martin [4] found $Q_{iA} \propto g^{-0.68}$. Balamuta and Golde [7] have reported branching fractions $f_A=0.54$ and $f_B=0.46$. Assuming the same velocity dependence for both channels

$$Q_q(g)=Q_{iA}(g)+Q_{iB}(g)=42.9/g^{0.78} , \quad (15)$$

where all cross sections are in $Å^2$ and g is in km/s. This result is compared with $Q_{\rm lim}$, Fig. 3.

Absolute energy-dependent quenching cross sections have been reported for Ar^*+H_2O over the energy range 45–125 meV[9]. The results were deconvoluted over the thermal velocity distribution and fitted to a function based on an approximate Landau-Zener collision model given by

$$Q_q(g)=B[1-e^{-\gamma/g}]g^{-2/3} , \quad (16)$$

where $B=104.4$ $Å^2$ $(\text{km/s})^{2/3}$ was computed from the London and dipole induced dipole interaction and 1.43 km/s was the best-fit value of the adjustable parameter γ. Quenching cross sections given by Eq. (16) are presented in Fig. 3. The results of earlier quenching measurements [2,3,5] are also shown. The Bourène and La Calvé and Velazco, Kolts, and Setser [5] measurements are for state selected Ar ($^3P_2$) and are averaged over a thermal distribution. These data are plotted in Fig. 3 at the average relative velocity. Some of the differences between $Q_{\rm lim}$ and the measured quenching cross sections may be due to anisotropy of the potential [19,24]. The potential anisotropy has been shown to increase the glory damping as velocity increases [25] and, referring to the measurements by Balamuta and Golde [7], Tabayashi and Shobatake [8], and Novicki and Krenos [9], $Q_{\rm lim}-Q_q$ does increase as velocity increases beyond 1.0 km/s.

VI. CONCLUSIONS

The present measurement indicates that, when averaged over all molecular orientations, the Ar^*+H_2O r^{-6}, r^{-8}, and r^{-10} long range potential terms can be represented as $r^{-6.17}$. Semiclassical analysis of the observed glory amplitude yields a potential-well minimum of 3.76 ± 0.09 meV located at a separation of 5.31 ± 0.13 Å. The observed attenuation of the glory amplitude gives an upper bound to the total inelastic cross section of 77 $Å^2$ at 1.0 km/s, which is above three of the five Ar^*+H_2O quenching measurements.

[1] M. A. A. Clyne, J. A. Coxon, D. W. Setser, and D. H. Stedman, Trans. Faraday Soc. **65**, 1177 (1969).
[2] M. Bourène and J. Le Calvé, J. Chem. Phys. **58**, 1452 (1973).
[3] J. W. Sheldon and E. E. Muschlitz, Jr., J. Chem. Phys. **68**, 5288 (1978).
[4] T. P. Parr and R. M. Martin, J. Phys. Chem. **82**, 2226 (1978).
[5] J. E. Velazco, J. H. Kolts, and D. W. Setser, J. Chem. Phys. **69**, 4357 (1978).
[6] H. L. Snyder, B. T. Smith, T. P. Parr, and R. M. Martin, Chem. Phys. **65**, 397 (1982).
[7] J. Balamuta and M. F. Golde, J. Chem. Phys. **76**, 2430 (1982).
[8] K. Tabayashi and K. Shobatake, J. Chem. Phys. **88**, 835 (1988).
[9] S. Novicki and J. Krenos, J. Chem. Phys. **89**, 7031 (1988).
[10] J. Bentley, J. Chem. Phys. **73**, 1805 (1980).
[11] M. Faubel and J. P. Toennies, Adv. At. Mol. Phys. **13**, 229 (1977).
[12] K. A. Hardy and J. W. Sheldon, Rev. Sci. Instrum. **52**, 1802 (1981).
[13] K. A. Hardy, E. Gillman, and J. W. Sheldon, J. Appl. Phys. **67**, 7240 (1990).
[14] M. E. Gersh, G. D. Sides, S. Y. Tang, and E. E. Muschlitz, Jr., J. Appl. Phys. **44**, 5356 (1973).
[15] P. Kusch, J. Chem. Phys. **40**, 1 (1964).
[16] N. C. Lang, H. V. Lilenfeld, and J. L. Kinsey, J. Chem. Phys. **55**, 3114 (1971).
[17] F. von Busch, Z. Phys. **193**, 412 (1966).
[18] H. Li, E. S. Gillman, J. W. Sheldon, and K. A. Hardy, Phys. Rev. A **45**, 225 (1991).
[19] E. R. Th. Kerstel, M. F. M. Janssens, K. A. H. Van Leeuwen, and H. C. W. Beijerinck, Chem. Phys. **119**, 325 (1988).
[20] L. D. Landau and E. M. Lifshitz, *Quantum Mechanics* (Pergamon, London, 1958).
[21] R. B. Bernstein and R. A. LaBudde, J. Chem. Phys. **58**, 1109 (1973).
[22] R. Shnidman, Nucl. Instrum. Methods **71**, 111 (1969).
[23] D. A. Micha, in *Modern Theoretical Chemistry,* edited by H. W. Miller (Plenum, New York, 1976), Vol. 2, p. 81.
[24] N. Hishinuma, Z. Phys. D **1**, 191 (1986).
[25] R. E. Olsen and R. B. Bernstein, J. Chem. Phys. **49**, 162 (1968).